IEEE Access
Multidisciplinary ⋮ Rapid Review ⋮ Open Access Journal

Received 6 May 2024, accepted 28 May 2024, date of publication 31 May 2024, date of current version 11 June 2024.

Digital Object Identifier 10.1109/ACCESS.2024.3407978

RESEARCH ARTICLE

Cost-Efficient Globalized Parameter Optimization of Microwave Components Through Response-Feature Surrogates and Nature-Inspired Metaheuristics

ANNA PIETRENKO-DABROWSKA[1,2], (Senior Member, IEEE), SLAWOMIR KOZIEL[2,1], (Fellow, IEEE), AND LUKASZ GOLUNSKI[1]

[1]Faculty of Electronics, Telecommunications and Informatics, Gdańsk University of Technology, 80-233 Gdańsk, Poland
[2]Engineering Optimization and Modeling Center, Department of Engineering, Reykjavik University, 102 Reykjavik, Iceland

Corresponding author: Anna Pietrenko-Dabrowska (anna.dabrowska@pg.edu.pl)

This work was supported in part by the Icelandic Research Fund under Grant 239858, and in part by the National Science Centre of Poland under Grant 2022/47/B/ST7/00072.

ABSTRACT Design of contemporary microwave devices predominantly utilizes computational models, including both circuit simulators and full-wave electromagnetic (EM) evaluation. The latter constitutes the sole generic way of rendering accurate assessment of the system outputs that considers phenomena such as cross-coupling or radiation and dielectric losses. Consequently, for reliability reasons, the final tuning of microwave device parameters is commonly performed utilizing EM simulation software. As EM analysis is computationally heavy, parametric optimization entails significant costs, also for local algorithms. The expenses generated by global search procedures are incomparably higher, and often prohibitive. Still, global optimization is more and more often necessary, for example, when re-designing a structure over extended ranges of operating conditions, if more than a single local optimum exists, or simply due to the absence of quality initial design. A possible workaround is surrogate-assisted optimization, yet a construction of accurate replacement models is a challenge by itself. This paper offers an innovative approach to a rapid globalized optimization of passive microwave components. It combines a machine learning procedure, specifically, an iterative construction and refinement of fast surrogates (with infill criterion being a minimization of the predictor-yielded objective improvement) with a response feature technology, where the metamodel targets suitably appointed characteristic points of the circuit outputs. These so-called response features are in a nearly linear relationship with the geometry parameters, which facilitates the search process and reduces the expenditures associated with surrogate model construction. Identification of the infill points is executed using a particle swarm optimization algorithm. Numerical experiments carried out using two microstrip circuits demonstrate the capability for a global search of the proposed algorithm, and its superior performance over direct nature-inspired-based optimization and surrogate-assisted search at the level of complete circuit characteristics. The original contributions of this work can be summarized as follows: (i) the development and implementation of the machine learning procedure that operates at the level of response features, (ii) the development of parameter space pre-screening stage employed to narrow down the region to be explored in the search process, (iii) demonstration of superiority of the proposed framework (including its remarkable computational efficiency) over a range of benchmark methods, both direct and surrogate-assisted ones.

INDEX TERMS EM-driven design, global optimization, microwave engineering, nature-inspired algorithms, response features, surrogate-assisted optimization.

The associate editor coordinating the review of this manuscript and approving it for publication was Qiang Li.

I. INTRODUCTION

The needs of emerging areas of high-frequency electronics, such as wireless communications [1], internet of things (IoT) [2], remote sensing [3], or wearable/implantable devices [4], [5], result in stringent performance demands imposed on microwave components designed for such applications. The required functionalities include reconfigurability [6], broadband [7] and multi-band applications [8], harmonic attenuation [9], non-standard phase responses [10], and—more and more often—limited physical dimensions [11], [12], [13], [14]. Meeting these demands lead to complex circuit geometries characterized by substantial numbers of parameters. In particular, miniaturization is often achieved by meandering the transmission lines [15] or incorporating compact microstrip resonant cells (CMRCs) [16], whereas harmonic suppression is achieved by employing additional filtering components or resonators [17], all of which have to be properly dimensioned. Furthermore, accurate evaluation of electrical characteristics of microwave devices calls for full-wave electromagnetic (EM) analysis to accommodate EM cross-coupling effects, radiation and dielectric losses, and the existence of connectors or other components (e.g., housing or installation fixtures in the case of antennas [18]). Thus, simulation-driven design optimization has become a must in the design of high-performance circuits. This includes the final stages of the design process (also referred to as design closure [19]), which involve refining geometry parameters, necessary to ensure the best attainable system performance.

EM-driven design is a practical necessity, yet it is a challenging process due to high computational expenditures it entails. Tuning of geometry parameters is associated with many system simulations, which can easily exceed a few hundred also for a local optimization (e.g., with numerical gradients) [20]. This translates into execution time reaching even up to several days. On the other hand, interactive approaches such as supervised parameter sweeping, continue to be extensively utilized both in academia and industry [21]. While formally cheaper, they are only capable of handling one or two parameters at a time, and, therefore, lead to sub-optimal results. Furthermore, an increasing number of design scenarios require global optimization, the cost of which is incomparably higher, and, in the case of microwave components, may be as high as over a week. The examples are plenty and include multimodal tasks (i.e., those featuring multiple local optima) such as optimization of coding metasurfaces [22], frequency selective surfaces [23] (as well as other metamaterial-based structures [24]), synthesis of radiation patterns of antenna arrays [25], [26], optimization of sparse [27] or conformal arrays [28], multi-criterial design [29]. Global search is also required if a sufficiently good starting point is unavailable (e.g., re-design of a filter or a compact coupler across a broad range of operating frequencies [30] or substrate parameters [31]), or the relationships between circuit dimensions and electrical characteristics are unintuitive (e.g., CMRC-based miniaturized circuits [32]).

The most employed techniques for global optimization constitute nature-inspired routines [33], [34], [35], commonly dubbed as metaheuristics [36]. Their operating principle is to mimic either biological [37] or social [38] processes, such as natural evolution [39], hunting or feeding strategies of various species [40], [41], etc. Nature-inspired methods process the sets of candidate solutions (populations, swarms, packs, etc.) [42], [43], which are referred to as individuals (particles, agents, etc.) [44]. These exchange information, which either affect their composition (crossover, mutation [45]), or their relocation in the parameter space (e.g., through randomized bias towards the individual/global best [46]). This arguably enables a global search capability, although at high computational costs, typically measured in thousands of objective function evaluations, and often rather poor repeatability of solutions. Some of the algorithms that fall into this this category include genetic [47] and evolutionary algorithms (GAs, EAs) [48], ant systems [49], differential evolution (DE) [50], particle swarm optimization (PSO) [51], firefly algorithm [52], grey wolf optimization [53], and numerous variations [25], [54], [55], [56], [102], [103], [104], [105], [106], [107], [108], [109], [110], [111]. However, the recent developments seem to be rather incremental, and novel algorithms often resemble some of the older techniques (e.g., PSO). One of the attractive features of nature-inspired routines is their straightforward handling and implementation. They are widely adopted for solving optimization tasks in the application areas, where evaluation of the objective function is given analytically or cheap to evaluate, e.g., mechanical structures described by low numbers of design variables [57], [58], [59], [60], [61], [62], [63], [64]. As mentioned earlier, due to poor computational efficiency, direct EM-driven metaheuristic-based optimization is normally prohibitive. The exceptions include cases where full-wave simulation is relatively cheap (up to 10-30 seconds per system evaluation), or analytical models are available. A flagship example of the latter is an analytical array factor model utilized for antenna array pattern synthesis [28].

Practical incorporation of population-based methods into EM-driven design can be realized using surrogate modelling techniques [65], [66]. This typically leads to iterative procedures where the metamodel serves as a predictor (to facilitate identifying the most propitious parts of the design space), and it is enhanced by adding EM simulation data acquired thus far [67]. Those additional data points are obtained using different infill criteria designed, e.g., to improve the model accuracy (e.g., maximization of mean squared error [68]), or to seek the optimum design (e.g., minimization of the merit function yielded by the predictor [69]). Procedures like these are often referred to as machine learning approaches [70], [71], [72], and some of the utilized modelling methods involve kriging [73],

Gaussian process regression (GPR) [74], artificial neural networks [75], [76], but also polynomial chaos expansion [77]. The major problem of surrogate-based nature-inspired methods is a rendition of the metamodel itself. Microwave components feature highly nonlinear (and multiple) frequency characteristics, representing of which requires large numbers of training data samples. Consequently, most algorithmic frameworks of this class are demonstrated using systems described by a few parameters, or problems defined over narrow parameter ranges [78], [79]. Some recent and computationally efficient surrogate-assisted approaches in high-frequency design can be found in [112], [113], [114], and [115]. Other recent studies concerning model- and optimization-based design have been reported in [116], [117], [118], [119], [120], [121], [122], [123], [124], and [125]. The issues associated with conventional data-driven modeling can be alleviated by means of performance-driven modelling methodologies [80], [81], [82], exploitation of multi-fidelity EM simulations [83], or a response feature technology [84]. The latter strategy relies on reformulating the design problem within the auxiliary space of characteristic points derived from the circuit's output. These points typically exhibit a weakly nonlinear relationship with the geometry parameters of the circuit [85]. This approach enables the creation of precise models using smaller training datasets.

In this study, we introduce an innovative algorithmic framework for limited-cost global optimization of passive microwave circuits. The search process is delegated to the response feature space spanned by the coordinates of key locations in the output curves, identified based on EM simulation data. The initial metamodel model is based on randomly allocated observables pre-selected to contain extractable features, and to ensure its sufficient accuracy. The additional points (frequently referred to as infill samples) are generated to minimize the predicted objective function (also formulated in terms of response features); the underlying search algorithm is a particle swarm optimizer. Operating in the domain of response features significantly reduces the CPU expenses of the search event and enhances its dependability as demonstrated using two microwave components. The average cost of global search is only about 140 EM simulations of the respective structure. This remarkably low cost, nearly ten times lower than that of population-based algorithms, has been attained through leveraging the problem-related knowledge, in particular, the characteristic points of the system outputs: both for observable pre-screening and generation of infill samples. Furthermore, the algorithm exhibits excellent success rate with satisfactory results produced during all algorithm runs. Thorough benchmarking against direct EM-driven nature-inspired optimization and a machine learning approach targeting circuit frequency characteristics demonstrates the superiority of the proposed technique in terms of both cost and reliability.

II. GLOBAL OPTIMIZATION OF MICROWAVE PASSIVES BY MEANS OF RESPONSE-FEATURE SURROGATES AND PROJECTED OBJECTIVE FUNCTION IMPROVEMENT

In this section of the paper, we delve into the specifics of the proposed optimization framework. We begin with the formulation of the microwave design problem in Section II-A, followed by an overview of the fundamentals of response features, or characteristic points, in Section II-B. The process of creating the initial surrogate model is discussed in Section II-C, while Section II-D elaborates on the core aspect of the algorithm: the infill point rendition by minimizing the projected objective function. In this step, the current surrogate model is optimized using a particle swarm optimization routine (as an example of a nature-inspired algorithm). The operation of the complete framework is summarized in Section II-E.

A. MICROWAVE DESIGN OPTIMIZATION

In this paper, we consider optimization of microwave components understood as the adjustment of parameters (typically, circuit dimensions) encapsulated in a vector $\boldsymbol{x}$, so that the operating parameters of the circuit are aligned with their target values, represented by a vector $\boldsymbol{F}_t$. The relevant notation has been gathered in Table 1. Table 2 provides examples of specific design tasks and defines the objective function $U(\boldsymbol{x}, \boldsymbol{F}_t)$, which quantifies the design quality regarding the vector $\boldsymbol{F}_t$. For microwave circuits, the electrical characteristics of interest are scattering parameters $S_{ij}(\boldsymbol{x}, f)$ (cf. Table 1) [86], as well as other quantities which may be estimated based on them, such as the phase response.

It should be noted that most of design problems feature several objectives, which are typically treated in different ways, either directly, or as design constraints [87]. Casting some of the goals into constraints is a convenient way of simplifying the problem and defining a scalar objective function. An alternative method is to combine design goals

TABLE 1. Design optimization of microwave components: Terminology.

Symbol	Meaning	Comment
$\boldsymbol{x} = [x_1 \ldots x_n]^T$	Vector of design parameters	Typically, the variables are geometry parameters (dimensions in mm)
$S_{ij}(\boldsymbol{x},f)$	Scattering parameters at the design $\boldsymbol{x}$ and frequency f	Subscripts i and j stand for the circuit ports
$F_t = [F_{t.1} \ldots F_{t.K}]^T$	Vector of target operating parameters	Examples: operating frequency (or frequencies for multi-band structures, power split ratio (in the case of couplers), bandwidth, substrate parameters (permittivity, thickness)
$U(\boldsymbol{x},\boldsymbol{F}_t)$	Objective function to be minimized in the design process	Function quantifying the design quality, cf. Table 2

TABLE 2. Design optimization of microwave components: Terminology.

Design task	Target vector	Objective function*
Circuit: Impedance matching transformer Objectives: Minimize maximum in-band reflection, operating band $F = [f_1\ f_2]$	$\boldsymbol{F}_t = [f_1\ f_2]^T$	$U(\boldsymbol{x}, \boldsymbol{F}_t) = U(\boldsymbol{x}, [f_1\ f_2]^T) = \max\{f \in [f_1\ f_2] : \lvert S_{11}(\boldsymbol{x}, f)\rvert\}$
Circuit: Microstrip coupler Objectives: • Minimize matching and isolation at the target operating frequency f_0 • Ensure the required power split K_P at f_0	$\boldsymbol{F}_t = [f_0\ K_P]^T$	$U(\boldsymbol{x}, \boldsymbol{F}_t) = U(\boldsymbol{x}, [f_0\ K_P]^T) =$ $= \max\{\lvert S_{11}(\boldsymbol{x}, f_0)\rvert, \lvert S_{41}(\boldsymbol{x}, f_0)\rvert\} +$ $+\beta\left[\lvert S_{21}(\boldsymbol{x}, f_0)\rvert - \lvert S_{31}(\boldsymbol{x}, f_0)\rvert - K_P\right]^2$
Circuit: Dual-band coupler Objectives: • Minimize matching and isolation at the operating frequencies f_1 and f_2 • Ensure equal power split at f_1 and f_2	$\boldsymbol{F}_t = [f_1\ f_2]^T$	$U(\boldsymbol{x}, \boldsymbol{F}_t) = U(\boldsymbol{x}, [f_1\ f_2]^T) = \max\{\lvert S_{11}(\boldsymbol{x}, f_1)\rvert, \lvert S_{11}(\boldsymbol{x}, f_2)\rvert,$ $\lvert S_{41}(\boldsymbol{x}, f_1)\rvert, \lvert S_{41}(\boldsymbol{x}, f_1)\rvert\}$ $+\beta[(\lvert S_{21}(\boldsymbol{x}, f_1)\rvert - \lvert S_{31}(\boldsymbol{x}, f_1)\rvert)^2$ $+(\lvert S_{21}(\boldsymbol{x}, f_2)\rvert - \lvert S_{31}(\boldsymbol{x}, f_2)\rvert)^2]$
Circuit: Compact rat-race coupler Objectives: • Minimize the footprint area $A(\boldsymbol{x})$ • Ensure equal power split at the operating frequency f_0 • Maintain $\lvert S_{11}\rvert$, $\lvert S_{41}\rvert \le -20$ dB over the bandwidth $[f_0 - B, f_0 + B]$	$\boldsymbol{F}_t = [f_0\ B]^T$	$U(\boldsymbol{x}, \boldsymbol{F}_t) = U(\boldsymbol{x}, [f_0\ B]^T) = A(\boldsymbol{x}) +$ $+\beta_1\left[\max\{c(\boldsymbol{x}) + 20, 0\}/20\right]^2$ $+\beta_2\left[\lvert S_{21}(\boldsymbol{x}, f_0)\rvert - \lvert S_{31}(\boldsymbol{x}, f_0)\rvert\right]^2$ where $c(\boldsymbol{x}) = \max\{f \in [f_0 - B, f_0 + B]:$ $\max\{\lvert S_{11}(\boldsymbol{x}, f)\rvert, \lvert S_{41}(\boldsymbol{x}, f)\rvert\}$
Circuit: Dual-band coupler Objectives: • Implement the circuit on the substrate of relative permittivity ε_r • Minimizes $\lvert S_{11}\rvert$ and $\lvert S_{41}\rvert$ at the operating frequencies f_1 and f_2 • Ensure equal power split at f_1 and f_2	$\boldsymbol{F}_t = [f_{0.1}\ f_{0.2}\ \varepsilon_r]^T$	$U(\boldsymbol{x}, \boldsymbol{F}_t) = U(\boldsymbol{x}, [f_1\ f_2\ \varepsilon_r]^T) =$ $= \max\{\lvert S_{11}(\boldsymbol{x}, f_1)\rvert, \lvert S_{41}(\boldsymbol{x}, f_1)\rvert, \lvert S_{11}(\boldsymbol{x}, f_2)\rvert, \lvert S_{41}(\boldsymbol{x}, f_2)\rvert\}$ $+\beta\left[\lvert S_{21}(\boldsymbol{x}, f_1)\rvert - \lvert S_{31}(\boldsymbol{x}, f_1)\rvert\right]^2$ $+\beta\left[\lvert S_{21}(\boldsymbol{x}, f_2)\rvert - \lvert S_{31}(\boldsymbol{x}, f_2)\rvert\right]$
Circuit: Triple-band power divider Objectives: • Ensure equal power split at the operating frequencies f_1, f_2, and f_3 • Minimize input matching $\lvert S_{11}\rvert$, output matching $\lvert S_{22}\rvert$ and $\lvert S_{33}\rvert$, and isolation $\lvert S_{23}\rvert$ at f_1, f_2, and f_3	$\boldsymbol{F}_t = [f_1\ f_2\ f_3]^T$	$U(\boldsymbol{x}, \boldsymbol{F}_t) = U(\boldsymbol{x}, [f_1\ f_2\ f_3]^T) = \max\{\max_{k,l\in\{1,2,3\}} \lvert S_{kk}(\boldsymbol{x}, f_l)\rvert,$ $\max_{l\in\{1,2,3\}} \lvert S_{23}(\boldsymbol{x}, f_l)\rvert\}$ $+\beta\sum_{l=1}^{3}(\lvert S_{21}(\boldsymbol{x}, f_l)\rvert - \lvert S_{31}(\boldsymbol{x}, f_l)\rvert)^2$

* The terms followed by β are penalty factors introduced to enforce the design constraints (e.g., required power split or matching/isolation bandwidth).

(e.g., a weighted sum method [88]), or explicit handling (multi-criterial design [89], [90], [91]), which are not considered in this work.

Having defined the objective function $U(\boldsymbol{x}, \boldsymbol{F}_t)$, the problem is posed as a non-linear task of the form

$$\boldsymbol{x}^* = \arg\min_{\boldsymbol{x}} U(\boldsymbol{x}, \boldsymbol{F}_t) \tag{1}$$

In (1), $\boldsymbol{x}^*$ is the optimum design to be identified.

B. RESPONSE FEATURES

Microwave parameter tuning is routinely conducted at the level of full-wave EM simulation models. On the one hand, this ensures adequate accuracy of evaluating the electrical characteristics. On the other hand, it is likely to inflate computational expenditures, which becomes a major problem when global optimization is of interest.

Global search allows for identification of the best possible design but requires exploring the entire design space. Needless to say, handling highly nonlinear characteristics of microwave components is a challenging endeavor. Consider Fig. 1 presenting an example of a branch-line coupler, as well as its responses (scattering parameters vs. frequency) at many randomly assigned designs. Clearly, global search is indispensable for optimization of the circuit to center its operation at, e.g., the exemplary target operating frequency of 0.6 GHz, because initiating local parameter tuning from majority of the points presented in Fig. 1(b) would fail.

A possible way of mitigating this problem offers a response feature approach [83] being found on reformulating the design task using appositely defined and extracted key (feature) points of the circuit outputs [85]. The dependence between dimensions and material parameters and the coordinates of feature points exhibits lower nonlinearity than an analogous dependence for the entire electrical responses, which has been extensively demonstrated in the literatures [84], [92], [93], and [94]. Consequently, the said reformulation effectively regularizes the design problem and enables achieving a faster convergence; thus, improves computational efficiency of the optimization processes [93]. In addition, it enables a reduction of the training dataset sizes when constructing surrogate models [94].

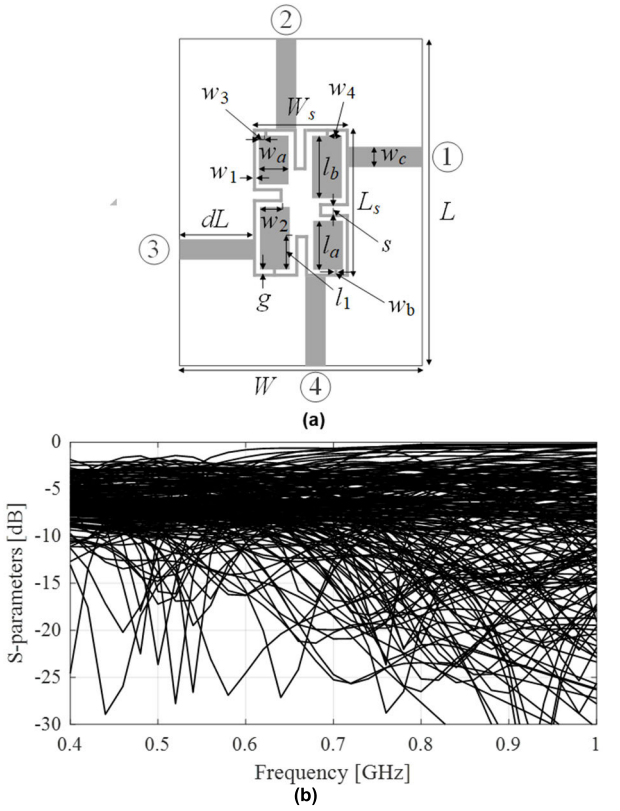

FIGURE 1. Exemplary branch-line coupler: (a) circuit geometry, (b) scattering parameters corresponding to random designs allocated over the assumed design space. Local optimization executed using the objective function such as those presented in Table 2 launched from most of designs of (b) would fail, thus global search is required.

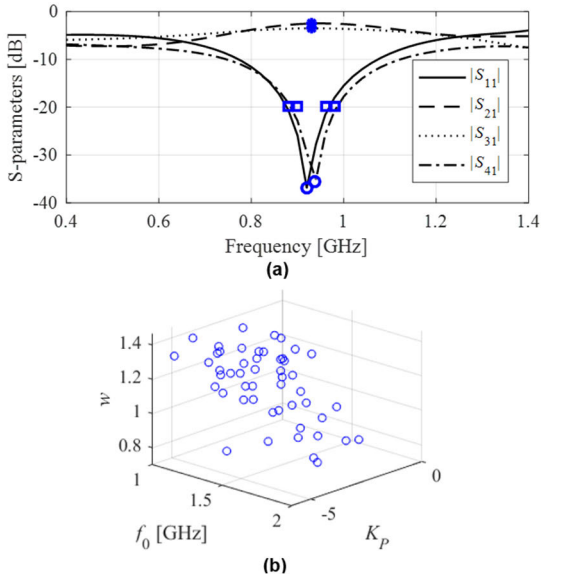

FIGURE 2. Branch-line coupler (see Fig. 1) and its response features: (a) exemplary choices of characteristic point: o – minimal levels of matching and isolation responses, ∗ – coordinates utilized for power division ratio assessment, □ – points referring to –20 dB values of $|S_{11}|$ and $|S_{41}|$; (b) interrelationship between power split ratio K_P (extracted from the response features) and one of the circuit's parameter rendered using randomly-generated designs.

The feature points are relevant to a specific problem at hand [82]. The main prerequisite is that the characteristic point set should enable to quantify the design objectives. If we consider, for example, a design of coupling structures for best matching and port isolation along with the target power split ratios, the feature points should account for the above operating parameters as well as the circuit's operating frequency. Figure 2 shows example definitions of the feature points that permit estimating the circuit's operational frequency, its power division ratio, along with –20 dB frequency band for the matching and isolation responses. Figure 2(b) demonstrates the less-nonlinear relationships between the coordinates of features and the selected component dimension (cf. [92], [93] for a more detailed discussion). These simple relationships greatly facilitate the parameter tuning process as well as a construction of a possible surrogate model that might be exploited to accelerate global optimization of the device. Both are the critical factors explored by the design framework proposed in this work.

We refer to the feature points of the considered device as $\boldsymbol{f}_P(\boldsymbol{x}) = [\boldsymbol{f}_F(\boldsymbol{x})^T \boldsymbol{f}_L(\boldsymbol{x})^T]^T$, where $\boldsymbol{f}_L(\boldsymbol{x}) = [f_{L.1}(\boldsymbol{x}) \ldots f_{L.k}(\boldsymbol{x})]^T$ is the vector of level coordinates, and the vector $\boldsymbol{f}_F(\boldsymbol{x}) = [f_{f.1}(\boldsymbol{x}) \ldots f_{f.k}(\boldsymbol{x})]^T$ comprises their frequency counterparts. For example, assuming four feature points for the coupler, two pertinent to the power division ratio (values of $|S_{31}|$ and $|S_{21}|$ at devices' operating frequency), and two pertinent to the minimum levels of the $|S_{11}|$ and $|S_{41}|$ characteristics, we would have

$$\boldsymbol{f}_f(\boldsymbol{x}) = \left[f_{f.1}(\boldsymbol{x}) \;\; f_{f.2}(\boldsymbol{x}) \;\; f_{f.3}(\boldsymbol{x}) \;\; f_{f.4}(\boldsymbol{x})\right]^T \quad (2)$$

$$\boldsymbol{f}_L(\boldsymbol{x}) = [f_{L.1}(\boldsymbol{x}) \;\; f_{L.2}(\boldsymbol{x}) \;\; f_{L.3}(\boldsymbol{x}) \;\; f_{L.4}(\boldsymbol{x})]^T \quad (3)$$

where $f_{f.1}$ and $f_{f.2}$ are frequencies of the minimal values of reflection $|S_{11}|$ and isolation $|S_{41}|$ responses, whereas $f_{L.1}$ and $f_{L.2}$ are the respective minima levels; further, $f_{f.3} = f_{f.4} = [f_{f.1} + f_{f.2}]/2 = f_0$ is the roughly estimated coupler's operating frequency, $f_{L.3}$ and $f_{L.4}$ are the values of $|S_{31}|$ and $|S_{41}|$ for f_0. Then we have $K_P = f_{L.3} - f_{L.4}$ (the estimated value of the power division ratio).

Further, $\boldsymbol{F}_o(\boldsymbol{x}) = F_o(\boldsymbol{f}_P(\boldsymbol{x}))$ will refer to the vector of device's operating parameters assessed based on response features $\boldsymbol{f}_P(\boldsymbol{x})$. Using this vector, the design problem reformulated regarding response features can be stated as

$$\boldsymbol{x}^* = \arg\min_{\boldsymbol{x}} U_F(\boldsymbol{x}, \boldsymbol{f}_P(\boldsymbol{x}), \boldsymbol{F}_t) \quad (4)$$

with the merit function U_F expressed analogously as presented in Table 2; however, using $\boldsymbol{F}_o(\boldsymbol{x})$, we may write compactly

$$U_F(\boldsymbol{x}, \boldsymbol{f}_P(\boldsymbol{x}), \boldsymbol{F}_t) = U_0(\boldsymbol{f}_P(\boldsymbol{x})) + \beta ||\boldsymbol{F}_o(\boldsymbol{f}_P(\boldsymbol{x})) - \boldsymbol{F}_t||^2 \quad (5)$$

where U_0 encodes the primary objective. As an illustration, if the aim is to relocate the operating frequency of a coupler structure to the target frequency f_t, achieve the

assumed power split error, and enhance matching and isolation at f_t, then, the primary objective would be to reduce $f_{L.1}$ and $f_{L.2}$, cf. (2), (3), i.e., we would define $U_0(\boldsymbol{f}_P(\boldsymbol{x})) = \max\{f_{L.1}(\boldsymbol{x}), f_{L.2}(\boldsymbol{x})\}$. The coefficient β controls the significance of the alignment of the operating parameters with the target as compared to the primary objective. Typically, we set $\beta = 100$.

C. CONSTRUCTING INITIAL SURROGATE MODEL

The proposed global optimization framework introduced in this work is based on a surrogate-assisted framework. The first step of the optimization process involves constructing an initial surrogate model. To minimize the number of training data samples required while ensuring adequate predictive capability, the model returns response features, as discussed in Section II-B. This surrogate, denoted as $\boldsymbol{s}^{(0)}(\boldsymbol{x})$, aims to capture the amplitude and frequency features' coordinates defined for the device under consideration

$$\boldsymbol{s}^{(0)}(\boldsymbol{x}) = \left[\left[s^{(0)}_{f.1}(\boldsymbol{x}) \ \ldots \ s^{(0)}_{f.K}(\boldsymbol{x})\right]^T \ \left[s^{(0)}_{L.1}(\boldsymbol{x}) \ \ldots \ s^{(0)}_{L.K}(\boldsymbol{x})\right]^T\right]^T \tag{6}$$

In this work, we use kriging interpolation [95] as the modelling method of choice. The training dataset consists of samples $\boldsymbol{x}_B^{(j)}$, $j = 1, \ldots, N_{init}$, and the vectors comprising features $\boldsymbol{f}_P(\boldsymbol{x}_B^{(j)})$, which are identified based on EM simulation data at the selected locations. The number N_{init} is not set beforehand, but it is adjusted so that the following two conditions are satisfied:

- It is possible to extract the feature points at all designs $\boldsymbol{x}_B^{(j)}$, $j = 1, \ldots, N_{init}$ (see Fig. 3);
- The accuracy of the model (here, the relative RMS error [80]) is sufficiently low, i.e., below the user-defined threshold, usually set to a few percent.

It should be noted that for certain designs featuring distorted responses (cf. Fig. 3), extraction of the response features is not possible, in which case the design would not be included into the training dataset. This procedure also acts as a pre-selection mechanism, which allows us to pinpoint the propitious parts of the parameter space and exclude other parts thereof by considering the knowledge identified from the system outputs expressed as the response features.

The dataset obtained under the two conditions mentioned earlier will be the basis of constructing an accurate metamodel, which can be applied to optimize the circuit at hand. Figure 4 summarizes the formal procedure of generating the sample points. Owing to the low-nonlinear dependence of the coordinates of features on geometry parameters of the device being optimized, the actual number of samples N_{init} is typically low, between fifty and a hundred. Moreover, the number of random observables that allow for obtaining N_{init} "good" samples will be larger, by a factor of 1.5 to perhaps up to three, depending on the problem complexity.

D. GENERATING INFILL POINTS THROUGH NATURE-INSPIRED OPTIMIZATION

The infill points are generated using the subsequent surrogate models, starting from the initial one, $\boldsymbol{s}^{(0)}$ (obtained as discussed in Section II-C), and the refined ones $\boldsymbol{s}^{(j)}$, $j = 1, 2, \ldots$. The surrogates act as predictors yielding the expected locations of the optimum design. The candidate vectors $\boldsymbol{x}^{(i+1)}$, $i = 0, 1, 2, \ldots$, are yielded by solving

$$\boldsymbol{x}^{(i+1)} = \arg\min_{\boldsymbol{x} \in X} U_F(\boldsymbol{x}, \boldsymbol{s}^{(i)}(\boldsymbol{x}), \boldsymbol{F}_t) \tag{7}$$

Problem (7) is formulated in the same way as (5); however, the characteristic points are predicted by means of the metamodel $\boldsymbol{s}^{(i)}$. The underlying search routine is the particle swarm optimizer (PSO) [97], the flagship bio-inspired procedure. It should be emphasized, however, that (7) can be solved using any global optimization method.

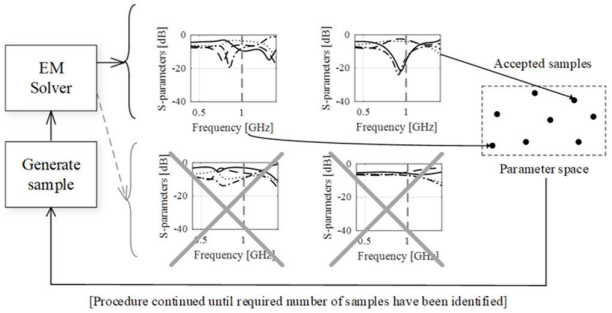

FIGURE 3. Sequential generation of training data points for constructing the initial metamodel: the operating frequencies of the accepted samples belong to the simulation frequency range.

1. Input parameters:
   - Design space X (interval $[\boldsymbol{l}\ \boldsymbol{u}]$, where $\boldsymbol{l}$ and $\boldsymbol{u}$ are lower and upper bounds for designable parameters; other constraints are possible per designer's needs);
   - Required modelling error E_{max};
2. Set $j = 0$;
3. Generate a sample $\boldsymbol{x}_{tmp} \in X$ using uniform probability distribution;
4. Evaluate circuit characteristics at $\boldsymbol{x}_{tmp}$ using EM analysis;
5. Extract the feature vector $\boldsymbol{f}_P(\boldsymbol{x}_{tmp})$; assign $\boldsymbol{f}_P(\boldsymbol{x}_{tmp}) = 0$ if features are not extractable (cf. Fig. 3);
6. **if** $||\boldsymbol{f}_P(\boldsymbol{x}_{tmp})|| > 0$
   Set $j = j + 1$;
   Set $\boldsymbol{x}_B^{(j)} = \boldsymbol{x}_{tmp}$;
   Construct surrogate model $\boldsymbol{s}_{tmp}(\boldsymbol{x})$ using dataset $\{\boldsymbol{x}_B^{(k)}, \boldsymbol{f}_P(\boldsymbol{x}_B^{(k)})\}_{k=1,\ldots,j}$;
   Estimate model error E_{tmp} using K-fold cross-validation [101], $K = \min\{j, 10\}$;
   if $E_{tmp} < E_{max}$
   Go to 8;
   end
   end
7. Go to 3;
8. Return $\boldsymbol{s}^{(0)}(\boldsymbol{x}) = \boldsymbol{s}_{tmp}(\boldsymbol{x})$;

FIGURE 4. Generating the training dataset for building initial surrogate model.

1. Input parameters:
   - Target operating frequencies $\boldsymbol{F}_t$ (cf. Section II.A);
   - Definition of the response features $\boldsymbol{f}_P$ and the objective function U_F (cf. Section II.B);
   - Design space X (interval [$\boldsymbol{l}$ $\boldsymbol{u}$], where $\boldsymbol{l}$ and $\boldsymbol{u}$ are lower and upper bounds for designable parameters);
   - Required modelling error E_{max};
   - Termination thresholds ε and $N_{no\_improve}$;
2. Generate the set of initial samples $\{\boldsymbol{x}_B^{(k)}, \boldsymbol{f}_P(\boldsymbol{x}_B^{(k)})\}_{k = 1,\ldots,Ninit}$, as described in Section II.C (cf. Fig. 4);
3. Construct initial surrogate model $\boldsymbol{s}^{(0)}(\boldsymbol{x})$;
4. Set $i = 0$;
5. Obtain infill point $\boldsymbol{x}^{(i+1)}$ by solving (4) using the PSO algorithm:
   $$\boldsymbol{x}^{(i+1)} = \arg\min_{\boldsymbol{x}\in X} U_F(\boldsymbol{x}, \boldsymbol{s}^{(i)}(\boldsymbol{x}), \boldsymbol{F}_t)$$
6. Update the dataset: $\{\boldsymbol{x}_B^{(k)}, \boldsymbol{f}_P(\boldsymbol{x}_B^{(k)})\}_{k = 1, \ldots, Ninit + i}$, with $\boldsymbol{x}_B^{(Ninit+j)} = \boldsymbol{x}^{(j)}$ for $j = 1, 2, \ldots$.
7. Set $i = i + 1$;
8. Construct the surrogate model $\boldsymbol{s}^{(i)}(\boldsymbol{x})$ using the updated dataset;
9. **if** $||\boldsymbol{x}^{(i)} - \boldsymbol{x}^{(i-1)}|| < \varepsilon$ OR no objective function improvement for $N_{no\ improve}$ iterations
   Go to 11;
   end
10. Go to 5;
11. Return $\boldsymbol{x}^* = \boldsymbol{x}^{(i)}$

FIGURE 5. Pseudocode of the developed algorithm for global microwave design optimization.

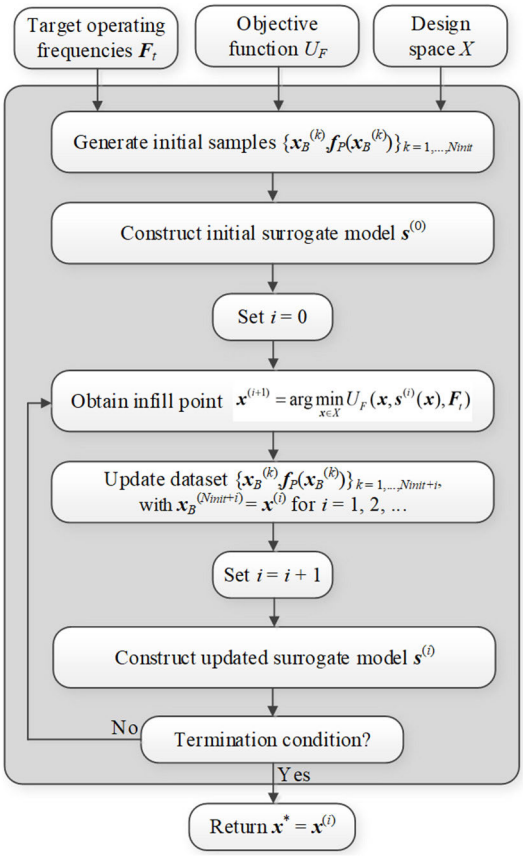

FIGURE 6. Flow chart of the developed algorithm for global optimization of microwave passive devices.

The problem itself is straightforward to solve owing to response feature formulation, and the employment of the regularization term in the cost function (cf. (5)). Meanwhile, massive evaluations of the cost function $U_F(\boldsymbol{x}, \boldsymbol{s}^{(i)}(\boldsymbol{x}), \boldsymbol{F}_t)$ can be carried out at negligible cost, therefore, utilization of the population-based methods would not deteriorate the computational efficacy of the optimization procedure.

Formally speaking, the infill criterion employed here leverages the predicted objective function improvement [98]. This means that we are not as much interested in improving the predictive power the metamodel but rather in exploitation of the region containing the optimum design (which was established beforehand through pre-screening). The EM-evaluated points accumulated during the optimization course is utilized to enhance the surrogate. More specifically, model $\boldsymbol{s}^{(j)}(\boldsymbol{x})$ constructed for the ith procedure's iteration is built using the dataset $\{\boldsymbol{x}_B^{(k)}, \boldsymbol{f}_P(\boldsymbol{x}_B^{(k)})\}_{k=1,\ldots,Njnit+j}$. Here, $\boldsymbol{x}_B^{(Nijit+j)} = x^{(j)}$ for $j = 1, 2, \ldots$.

The stopping condition of the search process consist in converging w.r.t. argument, i.e., $||x^{(j+1)} - \boldsymbol{x}^{(j)}|| < \varepsilon$ or when the cost function did not improve across the last $N_{no\_improwe}$ iterations. In the verification experiments of Section III, we use $N_{no\_improve} = 10$ and $\varepsilon = 10^{-2}$.

E. OPTIMIZATION ALGORITHM

The procedure for rendering the first metamodel, and the infill strategy of Section II-D are combined into an optimization framework summarized below. Table 3 gathers the control parameters. One can notice that solely three parameters exist: two related to the stopping criteria (i.e., allowing to modify the resolution of the search procedure). The third parameter imposes the requirements pertinent to the predictive power of the metamodel. Here, it is set to ten percent, which is a mild condition. Also, it is not tuned to the specific problem at hand, which is to demonstrate that the same algorithm setup can be used to solve a variety of design tasks.

TABLE 3. Control parameters and their explanation.

Parameter	Meaning	Default value
E_{max}	Maximum value of relative RMS error of the initial surrogate model (error estimated using cross-validation), cf. Section II.D	10%
ε	Termination threshold for convergence in argument, cf. Section II.D	10^{-2}
$N_{no\_improve}$	Termination threshold for no objective function value improvement, cf. Section II.D	10

The pseudocode outlining the optimization process is presented in Fig. 5, and the flow chart of the framework is shown in Fig. 7. The first stage is a generation of random samples and their pre-selection, leading to a rendition of the initial surrogate model (Steps 2 and 3). The infill points are obtained by optimizing the initial (for $i = 0$), and subsequent surrogates (for $i > 0$), as in Step 5. The refinement of the surrogate model is executed in Step 8 after updating the

training dataset (Step 6). The termination condition is determined in Step 9.

III. DEMONSTRATION EXAMPLES

For verification, we examine two microstrip devices, a compact rat-race coupler (RRC), and a dual-band power divider. Both structures are optimized using the algorithm introduced here, as well as several comparison techniques: (i) a multi-start local search, (ii) a particle swarm optimization routine (PSO), and (iii) a machine-learning-based procedure operating on the entire frequency responses of the circuits. Our primary focus is the dependability of the search procedure, described in terms of a relative number of algorithm executions that produce satisfactory designs (success rate), design quality, along with computational efficiency.

This part of the paper is commenced by introduction of the test circuits in Section III-A. Section III-B elaborates on the setup of the experiments. Section III-C discusses the results and summarizes our findings on the algorithm performance.

A. VERIFICATION CIRCUITS

The optimization procedure described in Section II is validated here with the use of two microstrip circuits: a compact rat-race coupler (RRC) with folded transmission lines (referred to as Circuit I) [99], and an equal-split dual-band power divider (Circuit II) [100]. The geometries of both circuits are depicted in Figs. 7(a) and 8(a), while Figs. 7(b) and 8(b) provide details about the relevant parameters (such as substrate and design variables) as well as the designable objectives. The EM evaluations of Circuits I and II are performed using CST Microwave Studio.

Circuit I is to work at the target frequency f_0, at which its impedance matching, and port isolation are to be improved as much as possible. Further, the power division ratio $|S_{31}| - |S_{21}|$ [dB] is to reach the target value K_P. For Circuit II, the purpose relies in minimization of matching and port isolation at the two centre frequencies f_1 and f_2, while ensuring equal power division. In this case, the second condition is satisfied due to the circuit symmetry, therefore, it is not explicitly tackled in the optimization event. For each circuit, we consider two design scenarios as specified in Table 4. The same table indicates the search space for both circuits in the form of the geometry parameter bounds. Note expansive variable ranges:

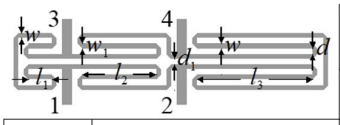

		Substrate	RO4003 (ε_r = 3.38, h = 0.76 mm)
		Design variables	$\boldsymbol{x} = [l_1\ l_2\ l_3\ d\ w\ w_1]^T$
Design goals	• Minimize matching $\lvert S_{11}\rvert$ and isolation $\lvert S_{41}\rvert$ at the operating frequency f_0 • Ensure power split ratio K_P	Other variables	$d_1 = d + \lvert w - w_1\rvert$, d = 1.0, w_0 = 1.7, l_0 = 15

FIGURE 7. Rat-race coupler using folded transmission lines (Circuit I) [99]: circuit topology and importand details.

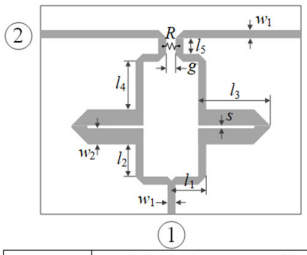

		Substrate	AD250 (ε_r = 2.5, h = 0.81 mm)
		Design variables	$\boldsymbol{x} = [l_1\ l_2\ l_3\ l_4\ l_5\ s\ w_2]^T$
Design goals	• Minimize input matching $\lvert S_{11}\rvert$, output matching $\lvert S_{22}\rvert$, $\lvert S_{33}\rvert$, and isolation $\lvert S_{23}\rvert$ at operating frequencies f_1 and f_2 • Ensure equal power split ratio	Other variables	w_1 = 2.2, g = 1

FIGURE 8. Dual-band equal-division power divider (Circuit II) [100]: circuit topology and importand details.

TABLE 4. Parameter spaces and design objectives for Circuits I and II.

Circuit	Target operating parameters: Symbols	Target operating parameters: Specific values for numerical experiments	Parameter space X (lower bounds $\boldsymbol{l}$ and upper bounds $\boldsymbol{u}$)
I	$\boldsymbol{F}_t = [f_0\ K_P]^T$	Case 1: f_0 = 1.8 GHz, K_P = –3 dB Case 2: f_0 = 1.2 GHz, K_P = 0 dB	$\boldsymbol{l}$ = [0.5 5.0 5.0 0.2 0.2 0.2]^T $\boldsymbol{u}$ = [15.0 30.0 50.0 2.0 2.0 2.0]^T
II	$\boldsymbol{F}_t = [f_1\ f_2]^T$	Case 1: f_1 = 3.0 GHz, f_2 = 4.8 GHz Case 2: f_1 = 2.0 GHz, f_2 = 3.3 GHz	$\boldsymbol{l}$ = [10.0 1.0 10.0 0.5 1.0 0.1 1.5]^T $\boldsymbol{u}$ = [40.0 20.0 40.0 15.0 6.0 1.5 8.0]^T

the mean ratio between upper and lower limits equals 13 Circuit I and it is 5 for Circuit II.

B. SETUP AND RESULTS

The control parameters of the developed procedure were adjusted as indicated in Table 3 ($E_{\max} = 10\%$, $\varepsilon = 10^{-2}$, and $N_{no\_improve} = 10$). The same setup is used for both circuits and all design scenarios. Table 5 summarizes the benchmark procedures that our method is compared to. These include three algorithms:

- A nature-inspired algorithm (here, PSO), which is to directly compare our framework with population-based approaches. Here, PSO is set with low computational budgets (two versions, with 500 and 1,000 objective function evaluations). This is to ensure that the optimization process does not incur excessive costs;
- A multiple-start gradient optimization, which allows us to showcase that the employed design problems are truly multi-modal, and, therefore, require global search approaches;
- A machine-learning-based algorithm, which is the procedure of Section II (kriging-based surrogate with infill criterion involving predicted objective function improvement), working with complete frequency characteristics of the circuit of interest. This method is

TABLE 5. Benchmark algorithms.

Algorithm	Algorithm type	Setup
I	Particle swarm optimizer (PSO)	Swarm size $N = 10$, standard control parameters ($\chi = 0.73$, $c_1 = c_2 = 2.05$); number of iterations set to 50 (version I) and 100 (version II)
II	Trust-region gradient based optimizer	Random initial design, response gradients estimated using finite differentiation, termination criteria based on convergence in argument and reduction of the trust region size
III	Machine learning algorithm (cf. Section II)	Algorithm similar to that of Section II: • Initial surrogate set up to ensure relative RMS error not higher than 10% with the maximum number of training samples equal to 400; • Optimization based on processing the antenna frequency characteristics (unlike response features in the proposed procedure); • Infill criterion: minimization of the projected objective function improvement [107].

TABLE 6. Circuit I: Results and benchmarking.

	Optimization algorithm	Performance figure: Average objective function value [dB]	Computational cost[$]	Success rate[#]
Case 1 f_0 = 1.8 GHz, K_P = –3	PSO (50 iterations)	–24.8	500	9/10
	PSO (100 iterations)	–34.0	1,000	10/10
	Trust-region algorithm	–18.7	102.8	6/10
	ML algorithm at the level of complete circuit responses	–32.8	485.3	10/10
	Proposed algorithm	–34.8	89.9	10/10
Case 2 f_0 = 1.2 GHz, K_P = 0	PSO (50 iterations)	–23.7	500	9/10
	PSO (100 iterations)	–36.2	1,000	10/10
	Trust-region algorithm	48.3	68.7	5/10
	ML algorithm at the level of complete circuit responses	–34.1	435.7	10/10
	Proposed algorithm	–43.9	106.3	10/10

[$] The cost in terms of the number of EM simulations of the circuit under design.
[#] Number of algorithms runs with the operating frequency allocated near the target.

considered to directly prove the advantages coming from employing the response feature technology.

Tables 6 and 7 display the numerical outcomes, while Figs. 9 through 12 depict the circuit responses at the ultimate designs acquired through the proposed algorithm. These figures also exhibit the dependence of the objective function value on the iteration index. Furthermore, Figures 13 and 14 illustrate the progression of the circuit design in the feature space, highlighting the changes in the power split ratio and operating frequency for Circuit I, and the operational frequencies for Circuit II. It can be noted that upon identifying the propitious region of the design space, the search process is focused on exploitation of that region, which was to be expected given the assumed infill criterion.

C. DISCUSSION

Here, we analyze the results provided in Table 6 and Table 7 and articulate our findings pertinent to the performance of the developed optimization procedure. The factors we are interested include dependability, the quality of the final designs rendered by the algorithms, their computational efficiency, as well as the benefits brought in by the response feature approach.

- Optimization process reliability: The results indicate that the developed procedure yields satisfactory designs (i.e., such that the resultant operating figures are close to the intended targets) in all algorithmic runs conducted during our experiments. In Tables 6 and 7, this is referred to as a success rate, which is 10/10 for the proposed method. As expected, the success rate for the multi-start gradient algorithm is significantly lower (about fifty percent on the average, but as low as 2/10 in Case 1 for Circuit II), which indicates that the test cases under consideration are multimodal, and their

TABLE 7. Circuit II: Results and benchmarking.

	Optimization algorithm	Performance figure: Average objective function value [dB]	Computational cost[$]	Success rate[#]
Case 1 f_1 = 3.0 GHz, f_2 = 4.8 GHz	PSO (50 iterations)	–19.6	500	8/10
	PSO (100 iterations)	–18.8	1,000	9/10
	Trust-region algorithm	–12.3	95.1	2/10
	ML algorithm at the level of complete circuit responses	–30.2	238.4	10/10
	Proposed algorithm	–32.8	194.4	10/10
Case 2 f_1 = 2.0 GHz, f_2 = 3.3 GHz dB	PSO (50 iterations)	–18.8	500	8/10
	PSO (100 iterations)	–19.7	1,000	9/10
	Trust-region algorithm	–20.6	93.8	7/10
	ML algorithm at the level of complete circuit responses	–22.5	273.2	10/10
	Proposed algorithm	–21.1	153.2	10/10

[$] The cost in terms of the number of EM simulations of the circuit under design.
[#] Number of algorithms runs with the operating frequency allocated near the target.

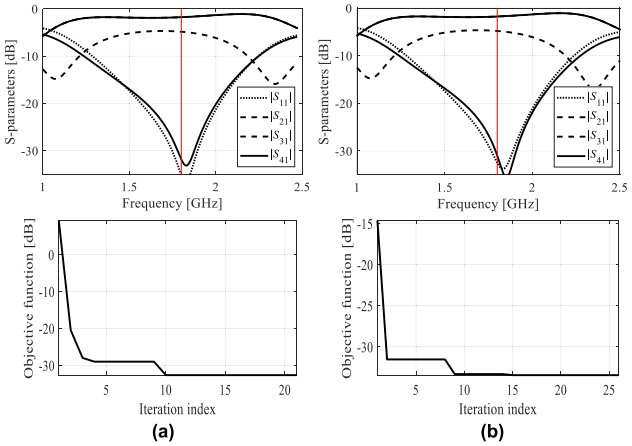

FIGURE 9. Circuit I: S-parameters at the optimal designs rendered by the developed procedure (top), along with objective function evolution (bottom). The results obtained in the representative algorithm instances for Case 1 are shown: (a) run 1, (b) run 2. The algorithm iterations are counted once the initial metamodel has been set up. Vertical line marks the intended operating frequency, here, 1.8 GHz.

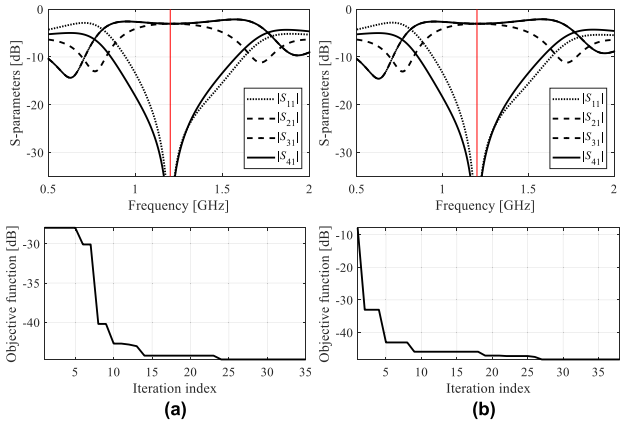

FIGURE 10. Circuit I: S-parameters at the optimal designs rendered by the developed procedure (top), along with objective function evolution (bottom). The results obtained in the representative algorithm instances for Case 2 are shown: (a) run 1, (b) run 2. The algorithm iterations are counted once the initial metamodel has been set up. Vertical line marks the intended operating frequency, here, 1.2 GHz.

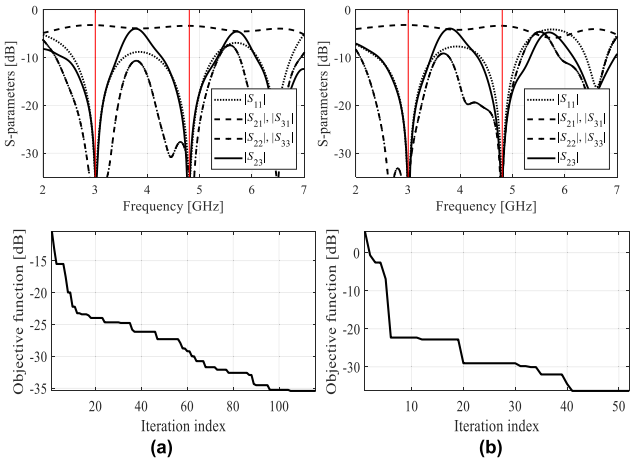

FIGURE 11. Circuit II: S-parameters at the optimal designs rendered by the developed procedure (top), along with objective function evolution (bottom). The results obtained in the representative algorithm instances for Case I are shown: (a) run 1, (b) run 2. The algorithm iterations are counted once the initial metamodel has been set up. Vertical line mark the intended operating frequencies, here, 3.0 GHz and 4.8 GHz.

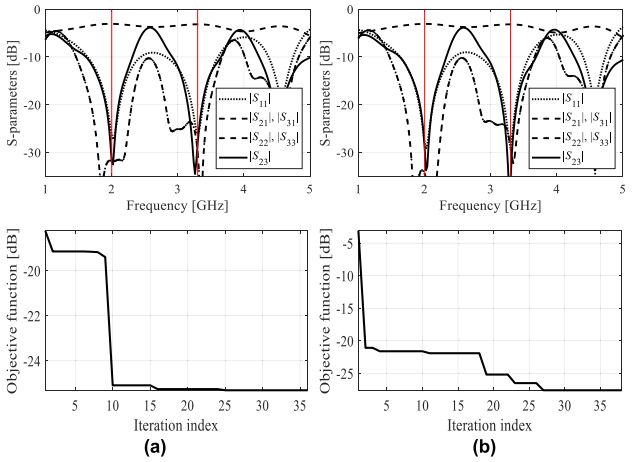

FIGURE 12. Circuit II: S-parameters at the optimal designs rendered by the developed procedure (top), along with objective function evolution (bottom). The results obtained in the representative algorithm instances for Case 2 are shown: (a) run 1, (b) run 2. The algorithm iterations are counted once the initial metamodel has been set up. Vertical line mark the intended operating frequencies, here, 2.0 GHz and 3.3 GHz.

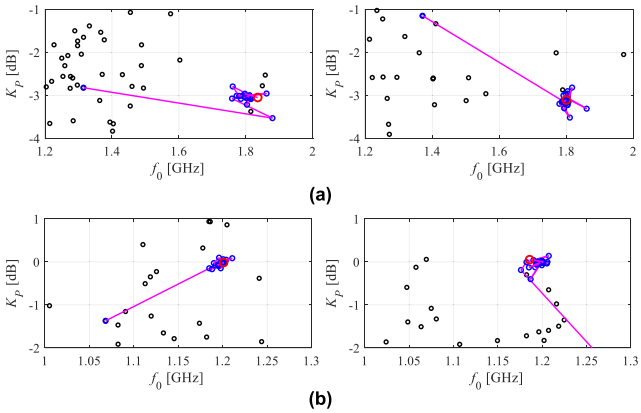

FIGURE 13. Circuit I: history of the optimization in the space of response features: (a) Case 1 (plot corresponding to the algorithm run shown in Fig. 9), (b) Case 2 (plot corresponding to the algorithm run shown in Fig. 10). Initial and infill samples are marked using black and blue dots, respectively; optimal solution shown using larger circle; optimization path represented by line segments illustrate the optimization path. Adjustment of the operating frequency range permitted capturing the optimization history near the optimal design.

successful handling does require global search methods. The reliability of the particle swarm optimizer is significantly higher with the success rate of 8/10 if the assumed computational resources equal 500 objective function evaluations, and 9/10 for 1,000. These numbers indicate that to achieve perfect success rate, the CPU budget would have to be increased, perhaps to 2,000 objective function evaluations or beyond. These levels of costs, however, are rather impractical. Finally, the machine learning algorithm directly operating on frequency responses of the circuits performs well in terms of design quality. The success rate is 10/10 for both circuits; yet, the CPU cost is much higher than for the proposed feature-based version.

- Design quality: The proposed procedure delivers solutions of similar or better objective function values to those produced by the benchmark methods. The numbers (way below –20 dB for Circuit I, and around –20 dB or so for Circuit II), indicate that the circuit matching and isolation characteristics are at satisfactory levels from the standpoint of practical applications, and (for Circuit I) the power split ratio reaches the target value (–3 dB for Case 1 and 0 dB for Case 2).
- Computational complexity: Apart from the local algorithm, which is considered to corroborate the necessity for global search for the test cases under consideration, the algorithm developed in this study exhibits the best computational efficiency. The average number

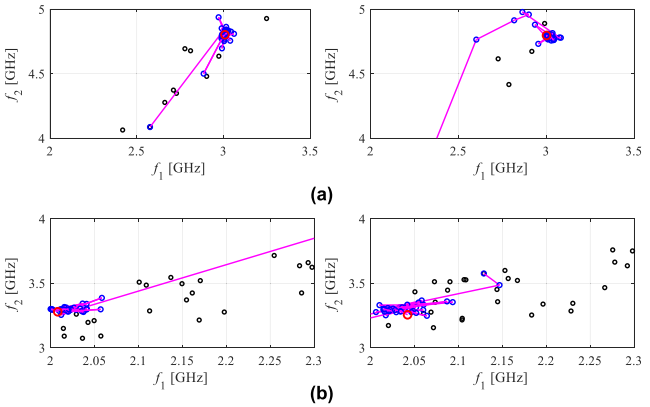

FIGURE 14. Circuit I: history of the optimization in the space of response features: (a) Case 1 (plot corresponding to the algorithm run shown in Fig. 11), (b) Case 2 (plot corresponding to the algorithm run shown in Fig. 12). Initial and ifill samples are marked using black and blue dots, respectively; optimal solution shown using larger circle; optimization path represented by line segments illustrate the optimization path. Adjustment of the operating frequency range permitted capturing the optimization history near the optimal design.

of circuit simulations is only 140, which is 86 percent lower than PSO, and almost seventy percent less than the machine learning procedure directly handling the frequency characteristics.

- The computational efficacy of the introduced algorithm is mainly achieved due to the incorporation of response features. This is particularly visible by comparing the number of training data points indispensable to establish the initial surrogate model, which is 76 and 81 for Circuit I (cases 1 and 2, respectively), and 69 and 73 for Circuit II. At the same time, constructing surrogates of similar predictive power at the level of complete frequency responses (as in the machine learning procedure), requires about 400 samples. As a matter of fact, the numbers would be higher, but 400 was set as the maximum computational cost of this phase of the optimization procedure.

The numerical results corroborate suitability of the proposed procedure as a low-cost substitution of the existing global optimization methods. It delivers consistent and repeatable results at the cost considerably lower than nature-inspired procedures, as well as machine learning methods that directly handle circuit responses. A potential limitation of our approach is associated with handling excessively large search spaces. More specifically, in such cases, the number of random observables necessary to identify a training dataset suitable for constructing the initial surrogate may be significant, as most of the samples would be rejected because of their poor quality (so that it would not be possible to extract their response features). On the other hand, in typical scenarios, the parameter spaces are set up based on engineering experience, which limits the likelihood of the these issues. It should also be recalled that the search spaces for the circuits of Figs. 7 and 8 are indeed large: the ratio of the upper to lower limits is around twelve on the average.

IV. CONCLUSION

This paper introduced a novel algorithmic framework for low-cost surrogate-based global optimization of microwave components. The proposed technique capitalizes on response-feature metamodels (here, kriging interpolation ones), built to represent the coordinates of suitably defined characteristic points of the device outputs, instead of the complete frequency responses. This does not only reduce the quantity of training data points necessary to render reliable surrogates, but also regularizes the functional landscape the optimization process operates on. The first stage of the search process is oriented towards a construction of the initial metamodel, using a collection of pre-selected random observables featuring extractable characteristic points. The second stage is iterative and consists of surrogate-based predictions and model refinement using the infill points accumulated along the optimization path. The criterion for allocating infill points consists in minimizing the modelled merit function, and we use the particle swarm optimizer (PSO) as the optimization routine of choice. Thus, the proposed algorithm falls into the category of machine learning frameworks. Comprehensive numerical validation, involving two microstrip circuits optimized for two sets of design specifications each, corroborates the excellent performance of the technique, better than that of a selection of benchmark methods. The latter include multi-start local search, population-based algorithms, and machine learning algorithm targeting entire frequency characteristics of the circuit at hand. The results indicate low computational cost of 140 EM analyses of the circuit per run on the average, perfect success rate (designs meeting the specs rendered by each run of the procedure), and high quality of the final designs as compared to the benchmark. An important benefit of incorporating the response feature technology is an excellent accuracy of the surrogate models constructed with the use of a limited number of training samples. Given the mentioned advantages, the developed methodology may be considered a feasible alternative for currently used global search techniques in the context of high-frequency design. One of the objectives of the future endeavors will be to extend the applicability range of our procedure to other types of microwave components (e.g., filters), and alternative the system outputs (e.g., phase characteristics), as well as EM-driven miniaturization.

The results obtained in this work can also suggest avenues for further research. An interesting topic would be investigation of possibilities of enhancing global search procedures in highly dimensional parameter spaces using the algorithmic tools developed in this study. The findings of our research, specifically very low cost of global search as compared to benchmark methods, are indicative of a potential of feature-based approaches in handling real-world problems associated with large number of parameters, which might be facilitated by inherent regularization offered by the feature-based methodologies. This would alleviate the major issue of machine learning frameworks, which is a construction of reliable surrogate model (hindered by both

the dimensionality issue and the extensive range of design variables). Another promising research direction is extending the concept of response features and their range of applicability to other types of microwave components, such as filters, resonator-based sensors, or metamaterial unit cells.

ACKNOWLEDGMENT

The authors would like to thank Dassault Systemes, France, for making CST Microwave Studio available.

REFERENCES

[1] R. K. Chandan and S. Pal, "Low SLL enhanced gain proximity coupled linear antenna array for 5G wireless communications," *AEU-Int. J. Electron. Commun.*, vol. 175, Feb. 2024, Art. no. 155081.

[2] D. Matos, M. D. da Cruz Jordão, R. Correia, and N. B. Carvalho, "Millimeter-wave BiCMOS backscatter modulator for 5 G-IoT applications," *IEEE Microw. Wireless Compon. Lett.*, vol. 31, no. 2, pp. 173–176, Feb. 2021.

[3] J. Wu, C. Zhang, H. Liu, and J. Yan, "Performance analysis of circular antenna array for microwave interferometric radiometers," *IEEE Trans. Geosci. Remote Sens.*, vol. 55, no. 6, pp. 3261–3271, Jun. 2017.

[4] R. Li, Y.-X. Guo, B. Zhang, and G. Du, "A miniaturized circularly polarized implantable annular-ring antenna," *IEEE Antennas Wireless Propag. Lett.*, vol. 16, pp. 2566–2569, 2017.

[5] M. Tekcin, S. Paker, and S. K. Bahadir, "UHF-RFID enabled wearable flexible printed sensor with antenna performance," *AEU-Int. J. Electron. Commun.*, vol. 157, Dec. 2022, Art. no. 154410.

[6] Y. Wu and H. Sun, "A low-profile wideband omnidirectional antenna with reconfigurable tri-polarization diversity," *AEU-Int. J. Electron. Commun.*, vol. 176, Mar. 2024, Art. no. 155149.

[7] M. Liu and F. Lin, "Two-section broadband couplers with wide-range phase differences and power-dividing ratios," *IEEE Microw. Wireless Compon. Lett.*, vol. 31, no. 2, pp. 117–120, Feb. 2021.

[8] R. Gómez-García, J. Rosario-De Jesus, and D. Psychogiou, "Multi-band bandpass and bandstop RF filtering couplers with dynamically-controlled bands," *IEEE Access*, vol. 6, pp. 32321–32327, 2018.

[9] B. Maity and S. K. Nayak, "Compact bowtie-shaped microstrip patch antennas with low cross-polarization and wideband harmonic suppression," *AEU-Int. J. Electron. Commun.*, vol. 168, Aug. 2023, Art. no. 154699.

[10] A. Ebrahimi, G. Beziuk, K. Ghorbani, and F. Martín, "Tunable phase shifters using composite inductive-capacitive loaded slow-wave transmission lines," *AEU-Int. J. Electron. Commun.*, vol. 148, May 2022, Art. no. 154155.

[11] Z. He and C. Liu, "A compact high-efficiency broadband rectifier with a wide dynamic range of input power for energy harvesting," *IEEE Microw. Wireless Compon. Lett.*, vol. 30, no. 4, pp. 433–436, Apr. 2020.

[12] Z. H. Jiang, M. D. Gregory, and D. H. Werner, "Design and experimental investigation of a compact circularly polarized integrated filtering antenna for wearable biotelemetric devices," *IEEE Trans. Biomed. Circuits Syst.*, vol. 10, no. 2, pp. 328–338, Apr. 2016.

[13] J. Kracek, M. Švanda, M. Mazanek, and J. Machac, "Implantable semi-active UHF RFID tag with inductive wireless power transfer," *IEEE Antennas Wireless Propag. Lett.*, vol. 15, pp. 1657–1660, 2016.

[14] L. Martinez, A. Belenguer, V. E. Boria, and A. L. Borja, "Compact folded bandpass filter in empty substrate integrated coaxial line at *S*-band," *IEEE Microw. Wireless Compon. Lett.*, vol. 29, no. 5, pp. 315–317, May 2019.

[15] T. Firmansyah, M. Alaydrus, Y. Wahyu, E. T. Rahardjo, and G. Wibisono, "A highly independent multiband bandpass filter using a multi-coupled line stub-SIR with folding structure," *IEEE Access*, vol. 8, pp. 83009–83026, 2020.

[16] S. Chen, M. Guo, K. Xu, P. Zhao, L. Dong, and G. Wang, "A frequency synthesizer based microwave permittivity sensor using CMRC structure," *IEEE Access*, vol. 6, pp. 8556–8563, 2018.

[17] Y. Zhu, J. Wang, J. Hong, J.-X. Chen, and W. Wu, "Two- and three-way filtering power dividers with harmonic suppression using triangle patch resonator," *IEEE Trans. Circuits Syst. I, Reg. Papers*, vol. 68, no. 12, pp. 5007–5017, Dec. 2021.

[18] D. Thangarasu, R. R. Thipparaju, and S. K. Palaniswamy, "Compound reconfigurable symmetric slotted MIMO antenna with ABS enclosure for indoor wireless applications," *AEU-Int. J. Electron. Commun.*, vol. 174, Jan. 2024, Art. no. 155059.

[19] A. Pietrenko-Dabrowska and S. Koziel, "Fast design closure of compact microwave components by means of feature-based metamodels," *Electronics*, vol. 10, no. 1, p. 10, Dec. 2020.

[20] J. Nocedal and S. J. Wright, *Numerical Optimization*, 2nd ed. New York, NY, USA: Springer, 2006.

[21] M. Cuevas, F. Pizarro, A. Leiva, G. Hermosilla, and D. Yunge, "Parametric study of a fully 3D-printed dielectric resonator antenna loaded with a metallic cap," *IEEE Access*, vol. 9, pp. 73771–73779, 2021.

[22] M. Abdullah and S. Koziel, "Supervised-learning-based development of multibit RCS-reduced coding metasurfaces," *IEEE Trans. Microw. Theory Techn.*, vol. 70, no. 1, pp. 264–274, Jan. 2022.

[23] Y. Li, P. Ren, and Z. Xiang, "A dual-passband frequency selective surface for 5G communication," *IEEE Antennas Wireless Propag. Lett.*, vol. 18, pp. 2597–2601, 2019.

[24] B. Blankrot and C. Heitzinger, "Efficient computational design and optimization of dielectric metamaterial structures," *IEEE J. Multiscale Multiphys. Comput. Techn.*, vol. 4, pp. 234–244, 2019.

[25] S. Liang, Z. Fang, G. Sun, Y. Liu, G. Qu, and Y. Zhang, "Sidelobe reductions of antenna arrays via an improved chicken swarm optimization approach," *IEEE Access*, vol. 8, pp. 37664–37683, 2020.

[26] M.-C. Tang, X. Chen, M. Li, and R. W. Ziolkowski, "Particle swarm optimized, 3-D-printed, wideband, compact hemispherical antenna," *IEEE Antennas Wireless Propag. Lett.*, vol. 17, pp. 2031–2035, 2018.

[27] H. Zhang, B. Bai, J. Zheng, and Y. Zhou, "Optimal design of sparse array for ultrasonic total focusing method by binary particle swarm optimization," *IEEE Access*, vol. 8, pp. 111945–111953, 2020.

[28] H. Li, Y. Jiang, Y. Ding, J. Tan, and J. Zhou, "Low-sidelobe pattern synthesis for sparse conformal arrays based on PSO-SOCP optimization," *IEEE Access*, vol. 6, pp. 77429–77439, 2018.

[29] J. E. Rayas-Sánchez, S. Koziel, and J. W. Bandler, "Advanced RF and microwave design optimization: A journey and a vision of future trends," *IEEE J. Microw.*, vol. 1, no. 1, pp. 481–493, Jan. 2021.

[30] M. Abdullah and S. Koziel, "A novel versatile decoupling structure and expedited inverse-model-based re-design procedure for compact single-and dual-band MIMO antennas," *IEEE Access*, vol. 9, pp. 37656–37667, 2021.

[31] S. Koziel and A. Pietrenko-Dabrowska, "On computationally-efficient reference design acquisition for reduced-cost constrained modeling and re-design of compact microwave passives," *IEEE Access*, vol. 8, pp. 203317–203330, 2020.

[32] H. Jin, Y. Zhou, Y. M. Huang, S. Ding, and K. Wu, "Miniaturized broadband coupler made of slow-wave half-mode substrate integrated waveguide," *IEEE Microw. Wireless Compon. Lett.*, vol. 27, no. 2, pp. 132–134, Feb. 2017.

[33] X. Li and K. M. Luk, "The grey wolf optimizer and its applications in electromagnetics," *IEEE Trans. Antennas Propag.*, vol. 68, no. 3, pp. 2186–2197, Mar. 2020.

[34] X. Luo, B. Yang, and H. J. Qian, "Adaptive synthesis for resonator-coupled filters based on particle swarm optimization," *IEEE Trans. Microw. Theory Techn.*, vol. 67, no. 2, pp. 712–725, Feb. 2019.

[35] A. Majumder, S. Chatterjee, S. Chatterjee, S. S. Chaudhari, and D. R. Poddar, "Optimization of small-signal model of GaN HEMT by using evolutionary algorithms," *IEEE Microw. Wireless Compon. Lett.*, vol. 27, no. 4, pp. 362–364, Apr. 2017.

[36] O. N. Oyelade, A. E. Ezugwu, T. I. A. Mohamed, and L. Abualigah, "Ebola optimization search algorithm: A new nature-inspired metaheuristic optimization algorithm," *IEEE Access*, vol. 10, pp. 16150–16177, 2022.

[37] S. Milner, C. Davis, H. Zhang, and J. Llorca, "Nature-inspired self-organization, control, and optimization in heterogeneous wireless networks," *IEEE Trans. Mobile Comput.*, vol. 11, no. 7, pp. 1207–1222, Jul. 2012.

[38] Q. Zhao and C. Li, "Two-stage multi-swarm particle swarm optimizer for unconstrained and constrained global optimization," *IEEE Access*, vol. 8, pp. 124905–124927, 2020.

[39] L. Jiacheng and L. Lei, "A hybrid genetic algorithm based on information entropy and game theory," *IEEE Access*, vol. 8, pp. 36602–36611, 2020.

[40] Z. Zhao, X. Wang, C. Wu, and L. Lei, "Hunting optimization: An new framework for single objective optimization problems," *IEEE Access*, vol. 7, pp. 31305–31320, 2019.

[41] Q. Zhang and L. Liu, "Whale optimization algorithm based on Lamarckian learning for global optimization problems," *IEEE Access*, vol. 7, pp. 36642–36666, 2019.

[42] P. Wang, Y. Rao, and Q. Luo, "An effective discrete grey wolf optimization algorithm for solving the packing problem," *IEEE Access*, vol. 8, pp. 115559–115571, 2020.

[43] Y. Meraihi, A. B. Gabis, S. Mirjalili, and A. Ramdane-Cherif, "Grasshopper optimization algorithm: Theory, variants, and applications," *IEEE Access*, vol. 9, pp. 50001–50024, 2021.

[44] A. A. K. Ismaeel, I. A. Elshaarawy, E. H. Houssein, F. H. Ismail, and A. E. Hassanien, "Enhanced elephant herding optimization for global optimization," *IEEE Access*, vol. 7, pp. 34738–34752, 2019.

[45] F. Liu, Y. Liu, F. Han, Y.-L. Ban, and Y. Jay Guo, "Synthesis of large unequally spaced planar arrays utilizing differential evolution with new encoding mechanism and Cauchy mutation," *IEEE Trans. Antennas Propag.*, vol. 68, no. 6, pp. 4406–4416, Jun. 2020.

[46] M. Kovaleva, D. Bulger, and K. P. Esselle, "Comparative study of optimization algorithms on the design of broadband antennas," *IEEE J. Multiscale Multiphys. Comput. Techn.*, vol. 5, pp. 89–98, 2020.

[47] H. Ghorbaninejad and R. Heydarian, "New design of waveguide directional coupler using genetic algorithm," *IEEE Microw. Wireless Compon. Lett.*, vol. 26, no. 2, pp. 86–88, Feb. 2016.

[48] D. Ding, Q. Zhang, J. Xia, A. Zhou, and L. Yang, "Wiggly parallel-coupled line design by using multiobjective evolutionay algorithm," *IEEE Microw. Wireless Compon. Lett.*, vol. 28, no. 8, pp. 648–650, Aug. 2018.

[49] D. Z. Zhu, P. L. Werner, and D. H. Werner, "Design and optimization of 3-D frequency-selective surfaces based on a multiobjective lazy ant colony optimization algorithm," *IEEE Trans. Antennas Propag.*, vol. 65, no. 12, pp. 7137–7149, Dec. 2017.

[50] C.-Y. Cui, Y.-C. Jiao, and L. Zhang, "Synthesis of some low sidelobe linear arrays using hybrid differential evolution algorithm integrated with convex programming," *IEEE Antennas Wireless Propag. Lett.*, vol. 16, pp. 2444–2448, 2017.

[51] V. Hosseini, Y. Farhang, K. Majidzadeh, and C. Ghobadi, "Customized mutated PSO algorithm of isolation enhancement for printed MIMO antenna with ISM band applications," *AEU-Int. J. Electron. Commun.*, vol. 145, Feb. 2022, Art. no. 154067.

[52] P. Baumgartner, T. Bauernfeind, O. Bíró, A. Hackl, C. Magele, W. Renhart, and R. Torchio, "Multi-objective optimization of Yagi–Uda antenna applying enhanced firefly algorithm with adaptive cost function," *IEEE Trans. Magn.*, vol. 54, no. 3, pp. 1–4, Mar. 2018.

[53] X. Li and Y.-X. Guo, "Multiobjective optimization design of aperture illuminations for microwave power transmission via multiobjective grey wolf optimizer," *IEEE Trans. Antennas Propag.*, vol. 68, no. 8, pp. 6265–6276, Aug. 2020.

[54] W. Li, Y. Zhang, and X. Shi, "Advanced fruit fly optimization algorithm and its application to irregular subarray phased array antenna synthesis," *IEEE Access*, vol. 7, pp. 165583–165596, 2019.

[55] Z. J. Jiang, S. Zhao, Y. Chen, and T. J. Cui, "Beamforming optimization for time-modulated circular-aperture grid array with DE algorithm," *IEEE Antennas Wireless Propag. Lett.*, vol. 17, pp. 2434–2438, 2018.

[56] Z. Bayraktar, M. Komurcu, J. A. Bossard, and D. H. Werner, "The wind driven optimization technique and its application in electromagnetics," *IEEE Trans. Antennas Propag.*, vol. 61, no. 5, pp. 2745–2757, May 2013.

[57] H. Ren, H. Ren, and Z. Sun, "HSFA: A novel firefly algorithm based on a hierarchical strategy," *Knowl.-Based Syst.*, vol. 279, Nov. 2023, Art. no. 110950.

[58] K. Wansasueb, S. Panmanee, N. Panagant, N. Pholdee, S. Bureerat, and A. R. Yildiz, "Hybridised differential evolution and equilibrium optimiser with learning parameters for mechanical and aircraft wing design," *Knowl.-Based Syst.*, vol. 239, Mar. 2022, Art. no. 107955.

[59] F. B. Ozsoydan and A. Baykasoglu, "A species-based flower pollination algorithm with increased selection pressure in abiotic local pollination and enhanced intensification," *Knowl.-Based Syst.*, vol. 225, Aug. 2021, Art. no. 107125.

[60] M.-Y. Cheng and M. N. Sholeh, "Optical microscope algorithm: A new metaheuristic inspired by microscope magnification for solving engineering optimization problems," *Knowl.-Based Syst.*, vol. 279, Nov. 2023, Art. no. 110939.

[61] X. Liu, X. Gao, Z. Wang, X. Ru, and Q. Zhang, "A metaheuristic causal discovery method in directed acyclic graphs space," *Knowl.-Based Syst.*, vol. 276, Sep. 2023, Art. no. 110749.

[62] C. Zhong, G. Li, and Z. Meng, "Beluga whale optimization: A novel nature-inspired metaheuristic algorithm," *Knowl.-Based Syst.*, vol. 251, Sep. 2022, Art. no. 109215.

[63] M. Abdel-Basset, R. Mohamed, S. A. A. Azeem, M. Jameel, and M. Abouhawwash, "Kepler optimization algorithm: A new metaheuristic algorithm inspired by Kepler's laws of planetary motion," *Knowl.-Based Syst.*, vol. 268, May 2023, Art. no. 110454.

[64] M. Dehghani, Z. Montazeri, E. Trojovská, and P. Trojovský, "Coati optimization algorithm: A new bio-inspired metaheuristic algorithm for solving optimization problems," *Knowl.-Based Syst.*, vol. 259, Jan. 2023, Art. no. 110011.

[65] Z. Zhang, Q. S. Cheng, H. Chen, and F. Jiang, "An efficient hybrid sampling method for neural network-based microwave component modeling and optimization," *IEEE Microw. Wireless Compon. Lett.*, vol. 30, no. 7, pp. 625–628, Jul. 2020.

[66] E. Van Nechel, F. Ferranti, Y. Rolain, and J. Lataire, "Model-driven design of microwave filters based on scalable circuit models," *IEEE Trans. Microw. Theory Techn.*, vol. 66, no. 10, pp. 4390–4396, Oct. 2018.

[67] A. I. J. Forrester and A. J. Keane, "Recent advances in surrogate-based optimization," *Prog. Aerosp. Sci.*, vol. 45, nos. 1–3, pp. 50–79, Jan. 2009.

[68] I. Couckuyt, F. Declercq, T. Dhaene, H. Rogier, and L. Knockaert, "Surrogate-based infill optimization applied to electromagnetic problems," *Int. J. RF Microw. Comput.-Aided Eng.*, vol. 20, no. 5, pp. 492–501, Sep. 2010.

[69] C. Chen, J. Liu, and P. Xu, "Comparison of parallel infill sampling criteria based on Kriging surrogate model," *Sci. Rep.*, vol. 12, no. 1, Jan. 2022, Art. no. 678.

[70] J. Tak, A. Kantemur, Y. Sharma, and H. Xin, "A 3-D-printed W-band slotted waveguide array antenna optimized using machine learning," *IEEE Antennas Wireless Propag. Lett.*, vol. 17, pp. 2008–2012, 2018.

[71] Q. Wu, H. Wang, and W. Hong, "Multistage collaborative machine learning and its application to antenna modeling and optimization," *IEEE Trans. Antennas Propag.*, vol. 68, no. 5, pp. 3397–3409, May 2020.

[72] N. Taran, D. M. Ionel, and D. G. Dorrell, "Two-level surrogate-assisted differential evolution multi-objective optimization of electric machines using 3-D FEA," *IEEE Trans. Magn.*, vol. 54, no. 11, pp. 1–5, Nov. 2018.

[73] S. Du, H. Liu, H. Yin, F. Yu, and J. Li, "A local surrogate-based parallel optimization for analog circuits," *AEU-Int. J. Electron. Commun.*, vol. 134, May 2021, Art. no. 153667.

[74] J. P. Jacobs, "Characterisation by Gaussian processes of finite substrate size effects on gain patterns of microstrip antennas," *IET Microw., Antennas Propag.*, vol. 10, no. 11, pp. 1189–1195, Aug. 2016.

[75] M. Ogut, X. Bosch-Lluis, and S. C. Reising, "A deep learning approach for microwave and millimeter-wave radiometer calibration," *IEEE Trans. Geosci. Remote Sens.*, vol. 57, no. 8, pp. 5344–5355, Aug. 2019.

[76] X. Yu, X. Hu, Z. Liu, C. Wang, W. Wang, and F. M. Ghannouchi, "A method to select optimal deep neural network model for power amplifiers," *IEEE Microw. Wireless Compon. Lett.*, vol. 31, no. 2, pp. 145–148, Feb. 2021.

[77] A. Petrocchi, A. Kaintura, G. Avolio, D. Spina, T. Dhaene, A. Raffo, and D. M. M.-P. Schreurs, "Measurement uncertainty propagation in transistor model parameters via polynomial chaos expansion," *IEEE Microw. Wireless Compon. Lett.*, vol. 27, no. 6, pp. 572–574, Jun. 2017.

[78] D.-K. Lim, K.-P. Yi, S.-Y. Jung, H.-K. Jung, and J.-S. Ro, "Optimal design of an interior permanent magnet synchronous motor by using a new surrogate-assisted multi-objective optimization," *IEEE Trans. Magn.*, vol. 51, no. 11, pp. 1–4, Nov. 2015.

[79] A. Toktas, D. Ustun, and M. Tekbas, "Multi-objective design of multi-layer radar absorber using surrogate-based optimization," *IEEE Trans. Microw. Theory Techn.*, vol. 67, no. 8, pp. 3318–3329, Aug. 2019.

[80] S. Koziel and A. Pietrenko-Dabrowska, *Performance-Driven Surrogate Modeling of High-Frequency Structures*. New York, NY, USA: Springer, 2020.

[81] S. Koziel, "Low-cost data-driven surrogate modeling of antenna structures by constrained sampling," *IEEE Antennas Wireless Propag. Lett.*, vol. 16, pp. 461–464, 2017.

[82] S. Koziel and A. Pietrenko-Dabrowska, "Performance-based nested surrogate modeling of antenna input characteristics," *IEEE Trans. Antennas Propag.*, vol. 67, no. 5, pp. 2904–2912, May 2019.

[83] A. Pietrenko-Dabrowska and S. Koziel, "Antenna modeling using variable-fidelity EM simulations and constrained co-kriging," *IEEE Access*, vol. 8, pp. 91048–91056, 2020.

[84] A. Pietrenko-Dabrowska and S. Koziel, "Generalized formulation of response features for reliable optimization of antenna input characteristics," *IEEE Trans. Antennas Propag.*, vol. 70, no. 5, pp. 3733–3748, May 2022.

[85] S. Koziel and A. Pietrenko-Dabrowska, "Expedited feature-based quasi-global optimization of multi-band antenna input characteristics with Jacobian variability tracking," *IEEE Access*, vol. 8, pp. 83907–83915, 2020.

[86] D. M. Pozar, *Microwace Engineering*, 4th ed. Hoboken, NJ, USA: Wiley, 2011.

[87] U. Ullah, S. Koziel, and I. B. Mabrouk, "Rapid redesign and bandwidth/size tradeoffs for compact wideband circular polarization antennas using inverse surrogates and fast EM-based parameter tuning," *IEEE Trans. Antennas Propag.*, vol. 68, no. 1, pp. 81–89, Jan. 2020.

[88] R. T. Marler and J. S. Arora, "The weighted sum method for multi-objective optimization: New insights," *Struct. Multidisciplinary Optim.*, vol. 41, no. 6, pp. 853–862, Jun. 2010.

[89] S. Mirjalili and J. S. Dong, *Multi-Objective Optimization Using Artificial Intelligence Techniques* (Springer Briefs in Applied Sciences and Technology). New York, NY, USA: Springer, 2019.

[90] J. K. Mandal, S. Mukhopadhyay, and P. Dutta, *Multi-Objective Optimization: Evolutionary to Hybrid Framework*. New York, NY, USA: Springer, 2018.

[91] S. Koziel and A. Pietrenko-Dabrowska, "Recent advances in accelerated multi-objective design of high-frequency structures using knowledge-based constrained modeling approach," *Knowl.-Based Syst.*, vol. 214, Feb. 2021, Art. no. 106726.

[92] S. Koziel and J. W. Bandler, "Reliable microwave modeling by means of variable-fidelity response features," *IEEE Trans. Microw. Theory Techn.*, vol. 63, no. 12, pp. 4247–4254, Dec. 2015.

[93] S. Koziel, "Fast simulation-driven antenna design using response-feature surrogates," *Int. J. RF Microw. Comput.-Aided Eng.*, vol. 25, no. 5, pp. 394–402, Jun. 2015.

[94] A. Pietrenko-Dabrowska and S. Koziel, "Simulation-driven antenna modeling by means of response features and confined domains of reduced dimensionality," *IEEE Access*, vol. 8, pp. 228942–228954, 2020.

[95] S. Koziel and A. Pietrenko-Dabrowska, "Recent advances in high frequency modeling by means of domain confinement and nested kriging," *IEEE Access*, vol. 8, pp. 189326–189342, 2020.

[96] G. C. Cawley and N. L. Talbot, "On over-fitting in model selection and subsequent selection bias in performance evaluation," *J. Mach. Learn. Res.*, vol. 11, pp. 2079–2107, Jul. 2010.

[97] V. Chandra and H. S. Anand, "Nature inspired meta heuristic algorithms for optimization problems," *Computing*, vol. 104, no. 2, pp. 251–269, Feb. 2022.

[98] J. Liu, Z. Han, and W. Song, "Comparison of infill sampling criteria in kriging-based aerodynamic optimization," in *Proc. 28th Int. Congr. Aeronaut. Sci.*, 2012, pp. 1–10.

[99] S. Koziel and A. Pietrenko-Dabrowska, "Reduced-cost surrogate modelling of compact microwave components by two-level Kriging interpolation," *Eng. Optim.*, vol. 52, no. 6, pp. 960–972, Jun. 2020.

[100] Z. Lin and Q.-X. Chu, "A novel approach to the design of dual-band power divider with variable power dividing ratio based on coupled-lines," *Prog. Electromagn. Res.*, vol. 103, pp. 271–284, 2010.

[101] A. R. Conn, N. I. M. Gould, P. L. Toint, *Trust Region Methods*. Philadelphia, PA, USA: SIAM, 2000.

[102] S. C. Shu, T. T. Wang, A. R. Yildiz, and J. S. Pan, "Ship rescue optimization: A new metaheuristic algorithm for solving engineering problems," *J. Internet Techn.*, vol. 25, no. 1, pp. 61–77, Jan. 2024.

[103] P. Mehta, S. M. Sait, B. S. Yıldız, M. U. Erdaş, M. Kopar, and A. R. Yıldız, "A new enhanced mountain gazelle optimizer and artificial neural network for global optimization of mechanical design problems," *Mater. Test.*, vol. 66, no. 4, pp. 544–552, Apr. 2024.

[104] Z. Meng, Q. Qian, M. Xu, B. Yu, A. R. Yıldız, and S. Mirjalili, "PINN-FORM: A new physics-informed neural network for reliability analysis with partial differential equation," *Comput. Methods Appl. Mech. Eng.*, vol. 414, Sep. 2023, Art. no. 116172.

[105] T. Kunakote, N. Sabangban, S. Kumar, G. G. Tejani, N. Panagant, N. Pholdee, S. Bureerat, and A. R. Yildiz, "Comparative performance of twelve metaheuristics for wind farm layout optimisation," *Arch. Comput. Methods Eng.*, vol. 29, no. 1, pp. 717–730, Jan. 2022.

[106] P. Mehta, B. S. Yildiz, S. M. Sait, and A. R. Yildiz, "Hunger games search algorithm for global optimization of engineering design problems," *Mater. Test.*, vol. 64, no. 4, pp. 524–532, Apr. 2022.

[107] B. S. Yıldız, S. Kumar, N. Pholdee, S. Bureerat, S. M. Sait, and A. R. Yildiz, "A new chaotic Lévy flight distribution optimization algorithm for solving constrained engineering problems," *Expert Syst.*, vol. 39, no. 8, Sep. 2022, Art. no. 312992.

[108] Z. Meng, B. S. Yıldız, G. Li, C. Zhong, S. Mirjalili, and A. R. Yildiz, "Application of state-of-the-art multiobjective metaheuristic algorithms in reliability-based design optimization: A comparative study," *Struct. Multidisciplinary Optim.*, vol. 66, no. 8, p. 191, Aug. 2023.

[109] S. Kumar, B. S. Yildiz, P. Mehta, N. Panagant, S. M. Sait, S. Mirjalili, and A. R. Yildiz, "Chaotic marine predators algorithm for global optimization of real-world engineering problems," *Knowl.-Based Syst.*, vol. 261, Feb. 2023, Art. no. 110192.

[110] B. S. Yıldız, S. Kumar, N. Panagant, P. Mehta, S. M. Sait, A. R. Yildiz, N. Pholdee, S. Bureerat, and S. Mirjalili, "A novel hybrid arithmetic optimization algorithm for solving constrained optimization problems," *Knowl.-Based Syst.*, vol. 271, Jul. 2023, Art. no. 110554.

[111] B. S. Yıldız, P. Mehta, N. Panagant, S. Mirjalili, and A. R. Yildiz, "A novel chaotic Runge Kutta optimization algorithm for solving constrained engineering problems," *J. Comput. Design Eng.*, vol. 9, no. 6, pp. 2452–2465, Dec. 2022.

[112] Z. Zhang, H. Chen, F. Jiang, Y. Yang, and Q. S. Cheng, "K-Means-Based multigroup differential evolution optimization framework for design of MIMO antenna with decoupling elements," *IEEE Antennas Wireless Propag. Lett.*, vol. 21, pp. 1980–1984, 2022.

[113] L. Xue, B. Liu, Y. Yu, Q. S. Cheng, M. Imran, and T. Qiao, "An unsupervised microwave filter design optimization method based on a hybrid surrogate model-assisted evolutionary algorithm," *IEEE Trans. Microw. Theory Techn.*, vol. 71, no. 3, pp. 1159–1170, Mar. 2023.

[114] Y. Yu, B. Liu, Y. Wang, and Q. S. Cheng, "Automated diplexer design with key performance indicator-based objectives," *IEEE Microw. Wireless Compon. Lett.*, vol. 32, no. 7, pp. 827–830, Jul. 2022.

[115] Z. Zhang, H. C. Chen, and Q. S. Cheng, "Surrogate-assisted quasi-Newton enhanced global optimization of antennas based on a heuristic hypersphere sampling," *IEEE Trans. Antennas Propag.*, vol. 69, no. 5, pp. 2993–2998, May 2021.

[116] A. Yan, R. Liu, J. Cui, T. Ni, P. Girard, X. Wen, and J. Zhang, "Designs of BCD adder based on Excess-3 code in quantum-dot cellular automata," *IEEE Trans. Circuits Syst. II, Exp. Briefs*, vol. 70, no. 6, pp. 2256–2260, May 2023.

[117] A. Yan, A. Cao, Z. Huang, J. Cui, T. Ni, P. Girard, X. Wen, and J. Zhang, "Two double-node-upset-hardened flip-flop designs for high-performance applications," *IEEE Trans. Emerg. Topics Comput.*, vol. 11, no. 4, pp. 1070–1081, Oct. 2023.

[118] Y. Guo, L. Wang, Z. Zhang, J. Cao, X. Xia, and Y. Liu, "Integrated modeling for retired mechanical product genes in remanufacturing: A knowledge graph-based approach," *Adv. Eng. Informat.*, vol. 59, Jan. 2024, Art. no. 102254.

[119] X. Xu and Z. Wei, "Dynamic pickup and delivery problem with transshipments and LIFO constraints," *Comput. Ind. Eng.*, vol. 175, Jan. 2023, Art. no. 108835.

[120] Y. Xie, X.-Y. Wang, Z.-J. Shen, Y.-H. Sheng, and G.-X. Wu, "A two-stage estimation of distribution algorithm with heuristics for energy-aware cloud workflow scheduling," *IEEE Trans. Services Comput.*, vol. 16, no. 6, pp. 4183–4197, Nov. 2023.
[121] B. Cao, J. Zhao, P. Yang, Y. Gu, K. Muhammad, J. J. P. C. Rodrigues, and V. H. C. de Albuquerque, "Multiobjective 3-D topology optimization of next-generation wireless data center network," *IEEE Trans. Ind. Informat.*, vol. 16, no. 5, pp. 3597–3605, May 2020.
[122] F. Ning, Y. Shi, X. Tong, M. Cai, and W. Xu, "Manufacturing cost estimation based on similarity," *Int. J. Comput. Integr. Manuf.*, vol. 36, no. 8, pp. 1238–1253, Aug. 2023.
[123] W. Liu, X. Bai, H. Yang, R. Bao, and J. Liu, "Tendon driven bistable origami flexible gripper for high-speed adaptive grasping," *IEEE Robot. Autom. Lett.*, vol. 9, no. 6, pp. 5417–5424, Jun. 2024.
[124] R. Wang, Q. Gu, S. Lu, J. Tian, Z. Yin, L. Yin, and W. Zheng, "FI-NPI: Exploring optimal control in parallel platform systems," *Electronics*, vol. 13, no. 7, p. 1168, Mar. 2024.
[125] W. Zheng, S. Lu, Y. Yang, Z. Yin, and L. Yin, "Lightweight transformer image feature extraction network," *PeerJ Comput. Sci.*, vol. 10, p. e1755, Jan. 2024.

ANNA PIETRENKO-DABROWSKA (Senior Member, IEEE) received the M.Sc. and Ph.D. degrees in electronic engineering from Gdańsk University of Technology, Poland, in 1998 and 2007, respectively. She is currently an Associate Professor with Gdańsk University of Technology. Her research interests include simulation-driven design, design optimization, control theory, modeling of microwave and antenna structures, and numerical analysis.

SLAWOMIR KOZIEL (Fellow, IEEE) received the M.Sc. and Ph.D. degrees in electronic engineering from Gdańsk University of Technology, Poland, in 1995 and 2000, respectively, and the M.Sc. degree in theoretical physics and the M.Sc. and Ph.D. degrees in mathematics from the University of Gdańsk, Poland, in 2000, 2002, and 2003, respectively. He is currently a Professor with the Department of Engineering, Reykjavik University, Iceland. His research interests include CAD and modeling of microwave and antenna structures, simulation-driven design, surrogate-based optimization, space mapping, circuit theory, analog signal processing, evolutionary computation, and numerical analysis.

LUKASZ GOLUNSKI received the M.Sc. degree in materials engineering and the Ph.D. degree in electronic engineering from Gdańsk University of Technology, Poland, in 2011 and 2018, respectively. He is currently an Assistant Professor with the Faculty of Electronics, Telecommunications and Informatics, Gdańsk University of Technology. His research interests include thin film growth, chemical vapor deposition and physical vapor methods, semiconductor diamond synthesis, and their electrical analysis.